ATLAS NOTE

ATLAS-CONF-2012-037

March 11, 2012

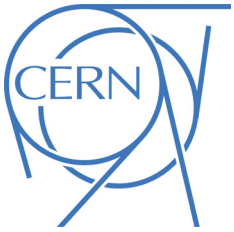

Hunt for new phenomena using large jet multiplicities and missing transverse momentum with ATLAS in $\mathcal{L} = 4.7\,\text{fb}^{-1}$ of $\sqrt{s} = 7$ TeV proton-proton collisions

The ATLAS Collaboration

Abstract

Results are presented of a search for new particles decaying to large numbers of jets in association with missing transverse momentum, using $4.7\,\text{fb}^{-1}$ of pp collision data at $\sqrt{s} = 7$ TeV collected by the ATLAS experiment in 2011. The event selection requires missing transverse momentum, no isolated electrons or muons, and from ≥6 to ≥9 jets. No evidence is found for physics beyond the Standard Model. The results are interpreted in the context of a MSUGRA/CMSSM supersymmetric model, where for large m_0, gluino masses smaller than 850 GeV are excluded at the 95% C.L., substantially extending previous limits. Within a simplified model containing only a gluino octet and a neutralino, values of the gluino mass smaller than 880 GeV are similarly excluded for neutralino masses less than 100 GeV.

1 Introduction

Many extensions of the Standard Model of particle physics predict the presence of TeV-scale strongly interacting particles that decay to lighter, weakly interacting descendants. Any such weakly interacting particles that are massive and stable can contribute to the dark matter content of the universe. The strongly interacting parents would be produced in the proton-proton interactions at the LHC, and would be characterized by events containing significant missing transverse momentum $E_{\mathrm{T}}^{\mathrm{miss}}$ from the unobserved weakly interacting daughters, and jets from emissions of quarks and/or gluons.

In the context of R-parity conserving [1, 2, 3, 4, 5] supersymmetry [5, 6, 7, 8, 9, 10], the strongly interacting parent particles are the squarks $\tilde{q}$ and gluinos $\tilde{g}$, they are produced in pairs, and the lightest supersymmetric particles are the stable dark matter candidates [11, 12]. Jets are produced from a variety of sources: from quark emission in supersymmetric cascade decays, production of heavy Standard Model particles (W, Z or t) which then decay hadronically, and from QCD radiation. Examples of particular phenomenological interest include models where squarks are significantly heavier than gluinos. In such models the gluino pair production and decay process

$$\tilde{g} + \tilde{g} \rightarrow \left(t + \bar{t} + \tilde{\chi}_1^0\right) + \left(t + \bar{t} + \tilde{\chi}_1^0\right)$$

can dominate, producing large jet multiplicities when the resulting top quarks decay hadronically. In the context of MSUGRA/CMSSM models, a variety of different cascade decays, including the $\tilde{g}\tilde{g}$ initiated process above, can lead to large jet multiplicities.

A previous ATLAS search in high jet multiplicity final states [13] examined data taken during the first half of 2011, corresponding to an integrated luminosity of $1.34\,\mathrm{fb}^{-1}$. This paper extends the analysis to the complete ATLAS 2011 pp data set, corresponding to $4.7\,\mathrm{fb}^{-1}$, and includes improvements in the analysis and event selection that further increase sensitivity to models of interest.

Events are selected with large jet multiplicities ranging from ≥ 6 to ≥ 9, in association with significant $E_{\mathrm{T}}^{\mathrm{miss}}$. Events containing high transverse momentum (p_{T}) electrons or muons are vetoed in order to reduce backgrounds from (semi-leptonically) decaying top quarks or W bosons. Other complementary searches have been performed by the ATLAS collaboration in final states with $E_{\mathrm{T}}^{\mathrm{miss}}$ and one or more leptons [14, 15]. Further searches have been performed by ATLAS using events with at least two, three or four jets [16], or with at least two b-tagged jets [17]. Searches have also been performed by the CMS collaboration, including a recent search in fully hadronic final states [18].

2 The ATLAS detector and data samples

The ATLAS experiment [19] is a multi-purpose particle physics detector with a forward-backward symmetric cylindrical geometry and nearly 4π coverage in solid angle.[1] The layout of the detector is dominated by four superconducting magnet systems, which comprise a thin solenoid surrounding inner tracking detectors and a barrel and two end-cap toroids supporting a large muon spectrometer. The calorimeters are of particular importance to this analysis. In the pseudorapidity region $|\eta| < 3.2$, high-granularity liquid-argon (LAr) electromagnetic (EM) sampling calorimeters are used. An iron-scintillator tile calorimeter provides hadronic coverage for $|\eta| < 1.7$. The end-cap and forward regions, spanning $1.5 < |\eta| < 4.9$, are instrumented with LAr calorimetry for both EM and hadronic measurements.

The data sample used in this analysis was taken during April – October 2011 with the LHC operating at a proton-proton centre-of-mass energy of $\sqrt{s} = 7$ TeV. Application of beam, detector and

[1] ATLAS uses a right-handed coordinate system with its origin at the nominal interaction point in the centre of the detector and the z-axis along the beam pipe. Cylindrical coordinates (r, ϕ) are used in the transverse plane, ϕ being the azimuthal angle around the beam pipe. The pseudorapidity η is defined in terms of the polar angle θ by $\eta = -\ln\tan(\theta/2)$.

data-quality requirements resulted in an integrated luminosity of $4.7 \pm 0.2\,\text{fb}^{-1}$ [20]. The analysis makes use of dedicated multi-jet triggers, the details of which changed during the data-taking period as a consequence of increasing LHC luminosity. The most selective of those triggers required at least four jets with $p_{\text{T}} > 45$ GeV or at least five jets with $p_{\text{T}} > 30$ GeV where the energy is measured at the electromagnetic scale.[2] In all cases the trigger efficiency was greater than 98% for events satisfying the offline jet multiplicity selections described later in Section 4.

3 Object reconstruction

Jet candidates are reconstructed using the anti-k_t jet clustering algorithm [21, 22] with radius parameter of 0.4. The inputs to this algorithm are clusters of calorimeter cells seeded by those with energy significantly above the measured noise. Jet momenta are constructed by performing a four-vector sum over these topological clusters of calorimeter cells, treating each as an $(E, \vec{p})$ four-vector with zero mass. The jet energies are corrected for the effects of calorimeter non-compensation and inhomogeneities by using p_{T}- and η-dependent calibration factors based on Monte Carlo (MC) simulations validated with extensive test-beam and collision-data studies [23]. Only jet candidates with $p_{\text{T}} > 20$ GeV and $|\eta| < 4.9$ are retained. Events are rejected if the correction applied to any jet candidate falling in problematic areas of the calorimeter provides a contribution to $E_{\text{T}}^{\text{miss}}$ that is greater than both 10 GeV and $0.1\,E_{\text{T}}^{\text{miss}}$. When identification of jets containing heavy flavour quarks is required, either to make measurements in control regions or for cross checks, a tagging algorithm exploiting both impact parameter and secondary vertex information is used. Jets are tagged for $|\eta| < 2.5$ and the parameters of the algorithm are chosen such that 70% of b-jets and $< 1\%$ of light flavour or gluon jets, are selected in $t\bar{t}$ events in Monte Carlo simulation [24]. Jets initiated by charm jets are tagged with about 20% efficiency.

Electron candidates are required to have $p_{\text{T}} > 20$ GeV and $|\eta| < 2.47$, and to satisfy the 'medium' electron shower shape and track selection criteria of Ref. [14]. Muon candidates are required to have $p_{\text{T}} > 10$ GeV and $|\eta| < 2.4$. Additional requirements are applied to muons when defining leptonic control regions. In this case muons must have longitudinal and transverse impact parameters within 1 mm and 0.2 mm of the primary vertex, respectively, and the sum of the transverse momentum of other tracks within a cone of $\Delta R = 0.2$ around the muon must be less than 1.8 GeV, where $\Delta R = \sqrt{(\Delta\eta)^2 + (\Delta\phi)^2}$.

The measurement of the missing transverse momentum two-vector $\vec{p}_{\text{T}}^{\,\text{miss}}$ and its magnitude (conventionally denoted $E_{\text{T}}^{\text{miss}}$) is then based on the transverse momenta of all electron and muon candidates, all jets which are not also electron candidates with $|\eta| < 4.5$, and all calorimeter clusters with $|\eta| < 4.5$ not associated to such objects [25].

Following the steps above, overlaps between candidate jets with $|\eta| < 2.8$ and leptons are resolved as follows. First, any such jet candidate lying within a distance $\Delta R < 0.2$ of an electron is discarded, then any lepton candidate remaining within a distance $\Delta R = 0.4$ of such a jet candidate is discarded. Thereafter, all jet candidates with $|\eta| > 2.8$ are discarded, and the remaining electron, muon and jet candidates are retained as reconstructed objects.

4 Event selection

Following the object reconstruction described in Section 3, events are discarded if they contain any jet failing quality criteria designed to suppress detector noise and non-collision backgrounds, or if they lack a reconstructed primary vertex with five or more associated tracks.

[2] The electromagnetic scale is the basic calorimeter signal scale for the ATLAS calorimeters. It has been established using test-beam measurements for electrons and muons to give the correct response for the energy deposited in electromagnetic showers, while it does not correct for the lower response of the calorimeter to hadrons.

Signal region	**7j55**	**8j55**	**9j55**	**6j80**	**7j80**	**8j80**
Isolated leptons (e, μ)	=0					
Jet p_T	>55 GeV			>80 GeV		
Jet $\|\eta\|$	<2.8					
Number of jets	≥ 7	≥ 8	≥ 9	≥ 6	≥ 7	≥ 8
$E_{\mathrm{T}}^{\mathrm{miss}}/\sqrt{H_T}$	>4 GeV$^{1/2}$					

Table 1: Definitions of the six signal regions.

For events containing no isolated electrons or muons, six non-exclusive signal regions (SRs) are defined as shown in Table 1. The first three require at least seven, eight or nine jets, respectively, with $p_{\mathrm{T}} > 55$ GeV; the latter three require at least six, seven or eight jets, respectively, with $p_{\mathrm{T}} > 80$ GeV. The final selection variable is $E_{\mathrm{T}}^{\mathrm{miss}}/\sqrt{H_{\mathrm{T}}}$, the ratio of the magnitude of the missing transverse momentum to the square root of the scalar sum H_{T} of the transverse momenta of all jets with $p_{\mathrm{T}} > 40$ GeV and $|\eta| < 2.8$. This ratio provides an estimate of the significance of the missing transverse momentum relative to the resolution due to stochastic variations in the measured jet energies [25]. The value of $E_{\mathrm{T}}^{\mathrm{miss}}/\sqrt{H_{\mathrm{T}}}$ is required to be larger than 4 GeV$^{1/2}$ for all signal regions.

No additional requirement is made on the separation between selected jets. The simple requirement an off-line jet multiplicity at least one larger than that used in the trigger achieves a high trigger efficiency ($> 98\%$) without the need to require any minimum jet-jet separation. Compared to Ref. [13], where jets were required to be separated by $\Delta R > 0.6$, the signal acceptance increases by a factor of two to five in the relevant region.

The dominant backgrounds are multi-jet production, including purely strong interaction processes and fully hadronic decays of $t\bar{t}$; semi- and fully-leptonic decays of $t\bar{t}$; and leptonically decaying W or Z bosons produced in association with jets. Non-fully-hadronic top, and W and Z are collectively referred to as 'leptonic' backgrounds, and can contribute to the signal regions when no e or μ leptons are produced (for example $Z \to \nu\nu$ or hadronic $W \to \tau\nu$ decays) or when they are produced but are outwith acceptance or fail reconstruction criteria. Contributions from gauge boson pair and single top quark production are negligible. The determination of the multi-jet and 'leptonic' backgrounds is described in Sections 6 and 7, respectively.

5 Monte Carlo simulations

Monte Carlo simulations are used to develop the analysis, as part of the 'leptonic' background determination process, and to assess sensitivity to specific SUSY signal models. The 'leptonic' backgrounds are generated using `Alpgen2.13` [26] with the PDF set `CTEQ6L1` [27]. Fully-leptonic $t\bar{t}$ events are generated with up to five additional partons in the matrix element, while semi-leptonic $t\bar{t}$ events are generated with up to three additional partons in the matrix element. W + jets and $Z \to \nu\bar{\nu}$ + jets are generated with up to six additional partons, and the $Z \to \ell^+\ell^-$ + jets (for $\ell \in \{e, \mu, \tau\}$) process is generated with up to five additional partons in the matrix element. In all cases, additional jets are generated via parton showering, which, together with fragmentation and hadronization, is performed by `HERWIG` [28, 29]. `JIMMY` [30] is used to simulate the underlying event.

Supersymmetric production processes are generated using `Herwig++2.4.2` [31]. Signal cross sections are calculated to next-to-leading order in the strong coupling constant, including the resummation

of soft gluon emission at next-to-leading-logarithmic accuracy (NLO+NLL) [32, 33, 34, 35, 36].[3] In all cases, an envelope of cross-section predictions is defined using the 68% C.L. ranges of the `CTEQ6.6` [37] (including the α_S uncertainty) and `MSTW2008 NLO` [38] PDF sets, together with independent variations of the factorisation and renormalisation scales by factors of two or one half. The nominal cross section value is taken to be the midpoint of the envelope and the uncertainty assigned is half the full width of the envelope, following closely the PDF4LHC recommendations [39]. For illustrative purposes, plots of kinematic quantities show the distribution expected for an example MSUGRA/CMSSM point, which has not been excluded in previous searches. This reference point is defined by[4]: $m_0 = 2960$ GeV, $m_{1/2} = 240$ GeV, $A_0 = 0$, $\tan\beta = 10$, and $\mu > 0$. MSUGRA/CMSSM particle spectra and decay modes are calculated with `ISAJET++7.75` [40].

All Monte Carlo samples employ a detector simulation [41] based on `GEANT4` [42] and are reconstructed with the same algorithms as the data.

6 Multi-jet backgrounds

The selection cuts were chosen such that the background from the multi-jet processes can be determined reliably from supporting measurements. In events dominated by jet activity, including hadronic decays of top quarks and gauge bosons, the $E_{\mathrm{T}}^{\mathrm{miss}}$ resolution is approximately proportional to $\sqrt{H_{\mathrm{T}}}$. The ratio $E_{\mathrm{T}}^{\mathrm{miss}}/\sqrt{H_{\mathrm{T}}}$ is therefore almost invariant under changes in the jet multiplicity. The multi-jet backgrounds are determined from data using control regions with lower $E_{\mathrm{T}}^{\mathrm{miss}}/\sqrt{H_{\mathrm{T}}}$ and/or lower jet multiplicity. The control regions are assumed to be dominated by Standard Model processes, an assumption that is corroborated by the agreement of multi-jet cross section measurements with up to six jets [43] with Standard Model predictions.

As an example, the prediction for the 8j55 signal region is obtained as follows. A template encapsulating the shape of the $E_{\mathrm{T}}^{\mathrm{miss}}/\sqrt{H_{\mathrm{T}}}$ distribution is obtained from those events that contain exactly six jets, using the same 55 GeV p_{T} threshold as the target signal region. That six-jet $E_{\mathrm{T}}^{\mathrm{miss}}/\sqrt{H_{\mathrm{T}}}$ template is normalised to the number of eight-jet events observed in the region $E_{\mathrm{T}}^{\mathrm{miss}}/\sqrt{H_{\mathrm{T}}} < 1.5$ GeV$^{1/2}$ after subtraction of the 'leptonic' background expectation. The normalized template then provides a prediction for the multi-jet background for the 8j55 signal region for which $E_{\mathrm{T}}^{\mathrm{miss}}/\sqrt{H_{\mathrm{T}}} > 4$ GeV$^{1/2}$.

Essentially the same procedure is used for each of the signal regions, and can be summarized as follows. For each jet p_{T} threshold $p_< \in \{55\ \mathrm{GeV}, 80\ \mathrm{GeV}\}$, control regions are defined for different numbers n_{jet} of jets found above $p_<$. The number of events $N_{p_<,n_{\mathrm{jet}}}(s_{\mathrm{min}}, s_{\mathrm{max}})$ for which $E_{\mathrm{T}}^{\mathrm{miss}}/\sqrt{H_{\mathrm{T}}}$ (in units of GeV$^{1/2}$) lies between s_{min} and s_{max} is determined, and the predicted 'leptonic' contributions $L_{p_<,n_{\mathrm{jet}}}(s_{\mathrm{min}}, s_{\mathrm{max}})$ subtracted

$$N^{\not L}_{p_<,n_{\mathrm{jet}}}(s_{\mathrm{min}}, s_{\mathrm{max}}) = N_{p_<,n_{\mathrm{jet}}}(s_{\mathrm{min}}, s_{\mathrm{max}}) - L_{p_<,n_{\mathrm{jet}}}(s_{\mathrm{min}}, s_{\mathrm{max}}).$$

Transfer factors

$$T_{p_<,n_{\mathrm{jet}}} = \frac{N^{\not L}_{p_<,n_{\mathrm{jet}}}(4, \infty)}{N^{\not L}_{p_<,n_{\mathrm{jet}}}(0, 1.5)}$$

[3] The NLL correction is used for squark and gluino production when the average of the squark masses in the first two generations and the gluino mass lie between 200 GeV and 2 TeV. In the case of gluino-pair (associated squark-gluino) production processes, the calculations were extended up to squark masses of 4.5 TeV (3.5 TeV). For masses outside this range and for other types of production processes (i.e. electroweak and associated strong and electroweak), cross sections at NLO accuracy obtained with `Prospino2.1` [32] are used.

[4] A particular MSUGRA/CMSSM model point is specified by five parameters: the universal scalar mass m_0, the universal gaugino mass $m_{1/2}$, the universal trilinear scalar coupling A_0, the ratio of the vacuum expectation values of the two Higgs fields $\tan\beta$, and the sign of the higgsino mass parameter μ.

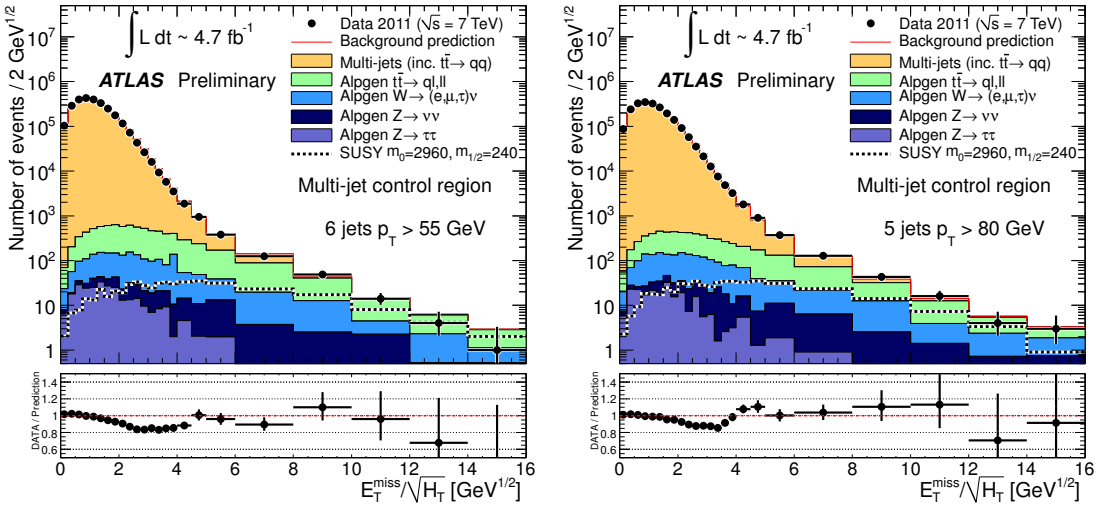

(a) **(b)**

Figure 1: $E_{\mathrm{T}}^{\mathrm{miss}}/\sqrt{H_{\mathrm{T}}}$ distributions in example multi-jet validation regions. **(a)** For exactly six jets with $p_{\mathrm{T}} > 55$ GeV, compared to a prediction based on the $E_{\mathrm{T}}^{\mathrm{miss}}/\sqrt{H_{\mathrm{T}}}$ distribution for exactly five jets with $p_{\mathrm{T}} > 55$ GeV. **(b)** For exactly five jets with $p_{\mathrm{T}} > 80$ GeV, compared to a prediction based on four jets with $p_{\mathrm{T}} > 80$ GeV. The multi-jet predictions have been normalized to the data in the region $E_{\mathrm{T}}^{\mathrm{miss}}/\sqrt{H_{\mathrm{T}}} < 1.5$ GeV$^{1/2}$ after subtraction of the predicted 'leptonic' backgrounds. The most important leptonic backgrounds are also shown, based on MC simulations. Variable bin sizes are used with bin width (in units of GeV$^{1/2}$) of 0.25 (up to 4), 0.5 (from 4 to 5), 1 (from 5 to 6), and then 2 thereafter.

connect regions with the same $p_<$ and n_{jet} with different $E_{\mathrm{T}}^{\mathrm{miss}}/\sqrt{H_{\mathrm{T}}}$. The multijet prediction for the signal region is found from the product of the $T_{p_<,n_{\mathrm{jet}}}$, with the same $p_<$ as the signal region and $n_{\mathrm{jet}} = 6$ when $p_< = 55$ GeV ($n_{\mathrm{jet}} = 5$ when $p_< = 80$ GeV) times the number of events (after subtracting the expected contribution from 'leptonic' background sources) satisfying signal region jet multiplicity requirements but with $E_{\mathrm{T}}^{\mathrm{miss}}/\sqrt{H_{\mathrm{T}}} < 1.5$ GeV$^{1/2}$.

6.1 Systematic uncertainties on multi-jet backgrounds

The method is validated by determining the accuracy of predictions for regions with jet multiplicities and/or $E_{\mathrm{T}}^{\mathrm{miss}}/\sqrt{H_{\mathrm{T}}}$ smaller than those chosen for the SRs. Figure 1 shows that the shape of the $E_{\mathrm{T}}^{\mathrm{miss}}/\sqrt{H_{\mathrm{T}}}$ distribution for $p_< = 55$ GeV and $n_{\mathrm{jet}} = 6$ is predicted to an accuracy of better than 20% from that measured using a template with the same value of $p_<$ and $n_{\mathrm{jet}} = 5$. Similarly the distribution for $p_< = 80$ GeV and $n_{\mathrm{jet}} = 5$ can be predicted for all $E_{\mathrm{T}}^{\mathrm{miss}}/\sqrt{H_{\mathrm{T}}}$ using a template with $n_{\mathrm{jet}} = 4$. The templates are normalised for $E_{\mathrm{T}}^{\mathrm{miss}}/\sqrt{H_{\mathrm{T}}} < 1.5$ GeV$^{1/2}$, and continue to provide a good prediction of the distribution out to values of $E_{\mathrm{T}}^{\mathrm{miss}}/\sqrt{H_{\mathrm{T}}}$ of 4 GeV$^{1/2}$ and beyond. Additional validation regions are defined for each $p_<$ and for jet multiplicity requirements equal to those of the signal regions, but for the intermediate values of $(s_{\mathrm{min}}, s_{\mathrm{max}})$ of (1.5, 2), (2, 2.5) and (2.5, 3.5). Residual inaccuracies in the predictions are used to quantify the systematic uncertainty from the closure of the method. Those uncertainties are in the range 15%-25%, depending on $p_<$ and $E_{\mathrm{T}}^{\mathrm{miss}}/\sqrt{H_{\mathrm{T}}}$.

The mean number of proton-proton interactions per bunch crossing $\langle\mu\rangle$ increased during the 2011 run, reaching $\langle\mu\rangle = 16$. To evaluate whether additional pp collisions contribute to the number of reconstructed jets, studies were performed of jet multiplicity as a function of $\langle\mu\rangle$ and of the number of reconstructed primary vertices. Further studies checked the consistency of the high-p_{T} tracks within selected jets with

a common primary vertex. It was found that while the effect of additional pile-up jets is significant for low-p_{T} jets, it is small for jets with $p_{\mathrm{T}} > 45$ GeV, and negligible for the jet selecton used for the SRs.

The presence of multiple in-time and out-of-time pp interactions also leads to a small but significant deterioration in the $E_{\mathrm{T}}^{\mathrm{miss}}$ resolution. The effectiveness of the $E_{\mathrm{T}}^{\mathrm{miss}}/\sqrt{H_{\mathrm{T}}}$ template method described above was tested separately for subsets of the data with different values of the instantaneous luminosity, and hence of $\langle\mu\rangle$. Good agreement was found separately for each subset of the data. Since the data set used to form the template has the same pileup conditions as that used to form the signal regions, the changing shape of the $E_{\mathrm{T}}^{\mathrm{miss}}$ resolution is included in the data-driven determination and does not lead to any additional systematic uncertainty.

Due to the presence of neutrinos produced in the decay of hadrons containing bottom or charm quarks, events with heavy-flavour jets exhibit a different $E_{\mathrm{T}}^{\mathrm{miss}}$ distribution. To quantify the systematic uncertainty associated with this difference, separate templates are defined for events with at least one b-tagged jet and for those with none. The sum of the predictions for events with and without b-tagged jets is compared to the flavour-blind approach, and the difference is used to characterize the systematic uncertainty from heavy flavour (10-20%). Other systematic uncertainties account for imperfect knowledge of: the subtracted 'leptonic' contributions (10%), the potential trigger inefficiency (2%), and imperfect response of the calorimeter in problematic areas (1%).

The backgrounds from multi-jet processes are cross checked using another data-driven technique [16] which smears the energies of individual jets from low-$E_{\mathrm{T}}^{\mathrm{miss}}$ multi-jet 'seed' events in data. Separate smearing functions are defined for b-tagged and non-b-tagged jets, with each modelling both the Gaussian core and the non-Gaussian tail of the jet response, including the loss of energy from unobserved neutrinos. The jet response functions are based on `GEANT4` [42] simulations [41]. The Gaussian core of the response is tuned to di-jet data, and the non-Gaussian tails are verified with data in three-jet control regions in which the $\vec{p}_{\mathrm{T}}^{\,\mathrm{miss}}$ can be associated with the fluctuation of a particular jet. The two methods agree within uncertainties, and so in what follows the prediction used is that based on $E_{\mathrm{T}}^{\mathrm{miss}}/\sqrt{H_{\mathrm{T}}}$ shape invariance.

7 'Leptonic' backgrounds

Backgrounds from non-fully-hadronic decays of $t\bar{t}$ + jets, W + jets and Z + jets are determined using Monte Carlo simulations that are normalized using control regions (CR) and cross checked in validation regions (VR). For each 'leptonic' background, control and validation regions are defined as shown in Table 2. By using control regions that are kinematically similar to the signal regions, theoretical uncertainties, including those arising from the use of a leading order (LO) generator, are reduced.

For those control regions where the Monte Carlo simulations predict at least one event for 4.7 fb^{-1}, the leptonic background prediction for each signal region is calculated by multiplying the number of data events found in the corresponding control region by a Monte Carlo-based factor. This transfer factor is defined to be the ratio of the number of MC events found in the signal region to the number of MC events found in the control region. In each case, the event counts are corrected for the expected contamination of the other background processes. Whenever less than one event is predicted in the control region, the Monte Carlo prediction for the corresponding signal region is used directly, without invoking a transfer factor.

For the $t\bar{t}$ + jets background, the validation region requires exactly one isolated muon, at least one b-tagged jet, and no selected electrons. The transverse mass for the muon transverse momentum $\vec{p}_{\mathrm{T}}^{\,\mu}$ and the missing transverse momentum two-vector $\vec{p}_{\mathrm{T}}^{\,\mathrm{miss}}$ is calculated in the massless approximation

$$m_{\mathrm{T}}^2 = 2|\vec{p}_{\mathrm{T}}^{\,\mu}||\vec{p}_{\mathrm{T}}^{\,\mathrm{miss}}| - 2\vec{p}_{\mathrm{T}}^{\,\mu} \cdot \vec{p}_{\mathrm{T}}^{\,\mathrm{miss}} ,$$

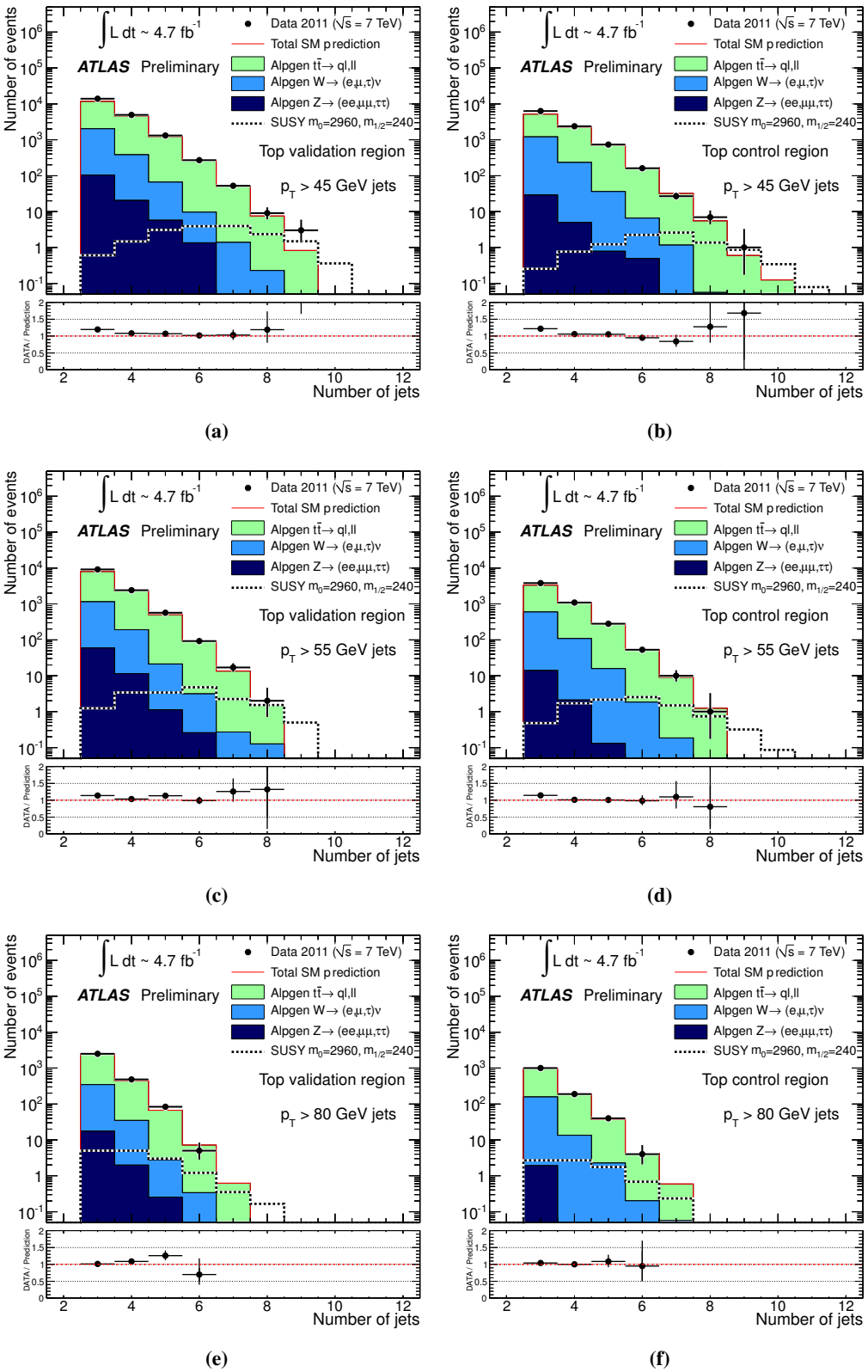

Figure 2: Jet multiplicity distributions for the $t\bar{t}$ + jets validation regions (left) and control regions (right) before any jet multiplicity requirements, for a jet p_{T} threshold of 45 GeV (top), 55 GeV (middle) and 80 GeV (bottom).

	$t\bar{t}$ + jets	W + jets	Z + jets
Muon kinematics	$p_{\mathrm{T}} > 20$ GeV, $\lvert\eta\rvert < 2.4$		
Muon multiplicity	= 1		= 2
Electron multiplicity	= 0		
b-tag jets	≥ 1	= 0	—
m_{T} or $m_{\mu\mu}$	50 GeV $< m_{\mathrm{T}} <$ 100 GeV		80 GeV $< m_{\mu\mu} <$ 100 GeV
VR $\rightarrow$ CR transform	$\mu \rightarrow$ jet		$\mu \rightarrow \nu$
Jet p_{T}, $\lvert\eta\rvert$, multiplicity (CR)	As in Table 1.		
$E_{\mathrm{T}}^{\mathrm{miss}} / \sqrt{H_{\mathrm{T}}}$ (CR)			

Table 2: Definitions of the validation regions and control regions for the 'leptonic' backgrounds: $t\bar{t}$ + jets, W + jets and Z + jets. The validation regions VR are defined by the first five selection requirements. A long dash '—' indicates that no requirement is made. The control regions CR differ from the VR in their treatment of the muons, and by having additional requirements on jets and $E_{\mathrm{T}}^{\mathrm{miss}} / \sqrt{H_{\mathrm{T}}}$, as shown in the final two rows.

and must satisfy 50 GeV $< m_{\mathrm{T}} <$ 100 GeV. Figure 2 shows the jet multiplicity in the $t\bar{t}$ validation regions, and it is demonstrated that the Monte Carlo provides a good description of the data.

The $t\bar{t}$ control regions used to calculate the background expectation differ from the validation regions as follows. Since the dominant source of background is from hadronic τ decays in the control regions, the muon is used to mimic a jet, as follows. If the muon has sufficient p_{T} to pass the jet selection threshold $p_{<}$, the jet multiplicity is incremented by one. If the muon p_{T} is larger than 40 GeV it is added to H_{T}. The selection variable $E_{\mathrm{T}}^{\mathrm{miss}} / \sqrt{H_{\mathrm{T}}}$ is then recalculated, and required to be larger than the threshold value of 4 $\mathrm{GeV}^{1/2}$. Distributions of the jet multiplicity in the $t\bar{t}$ control regions may also be found in Figure 2.

The W + jets validation regions and control regions are defined in a similar manner to those for $t\bar{t}$ + jets, except that a b-jet veto is used rather than a b-jet requirement (see Table 2). Figure 3 shows that the resulting jet multiplicity distributions are well described by the Monte Carlo simulations.

The Z + jets validation regions are defined (as shown in Table 2) requiring precisely two muons with invariant mass $m_{\mu\mu}$ consistent with m_Z. The dominant backgrounds from Z + jets arise from decays to neutrinos, so in forming the Z + jets control regions from the validation regions, the vector sum of the $\vec{p}_{\mathrm{T}}$ of the muons is added to the measured $\vec{p}_{\mathrm{T}}^{\,\mathrm{miss}}$, to model the $E_{\mathrm{T}}^{\mathrm{miss}}$ expected from $Z \rightarrow \nu\nu$ events. The selection variable $E_{\mathrm{T}}^{\mathrm{miss}} / \sqrt{H_{\mathrm{T}}}$ is then recalculated and required to be greater than 4 $\mathrm{GeV}^{1/2}$ for events in the control region. Figure 4 shows that the resulting jet multiplicity distributions in both validation and control regions are well described by the Monte Carlo simulations.

For each of the 'leptonic' backgrounds further comparisons are made between Monte Carlo and data using the lower jet p_{T} threshold of 45 GeV, showing agreement within uncertainties for all multiplicities (up to nine jets for $t\bar{t}$, see Figure 2 a and b). The `ALPGEN` Monte Carlo predictions for Z + jets and W + jets were determined with six additional partons in the matrix element calculation, and cross checked with a calculation in which only five additional partons were produced in the matrix element – in each case with additional jets being produced in the parton shower. The two predictions are consistent with each other and with the data, providing further supporting evidence that the parton shower offers a sufficiently accurate description of the additional jets.

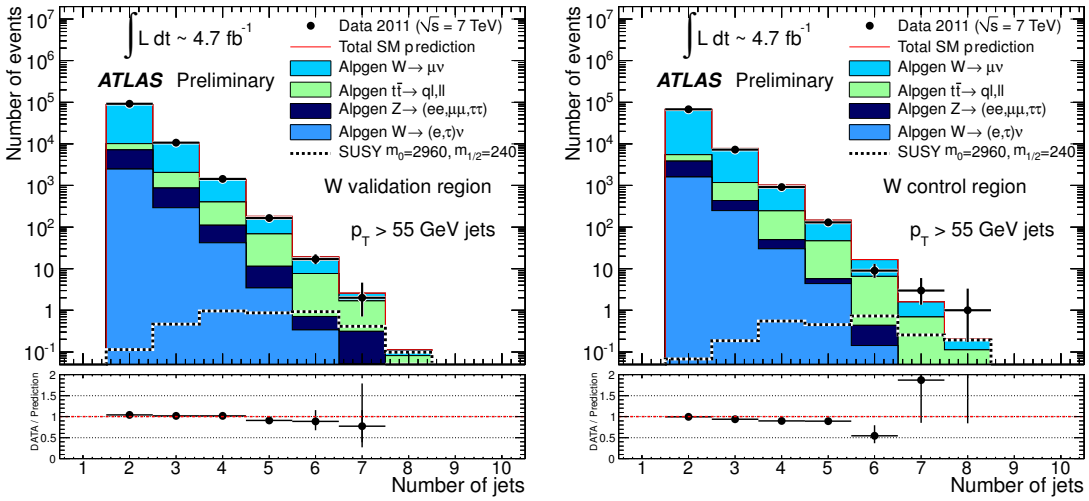

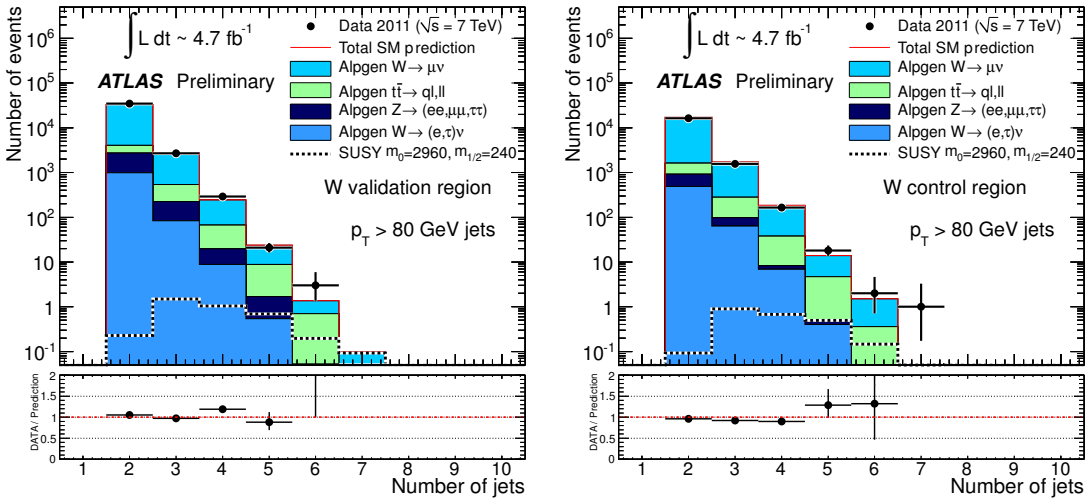

Figure 3: Jet multiplicity distributions for the $W^{\pm}$ + jets validation regions (left) and control regions (right) before any jet multiplicity requirements, and for a jet p_{T} threshold of 55 GeV (top) and 80 GeV (bottom).

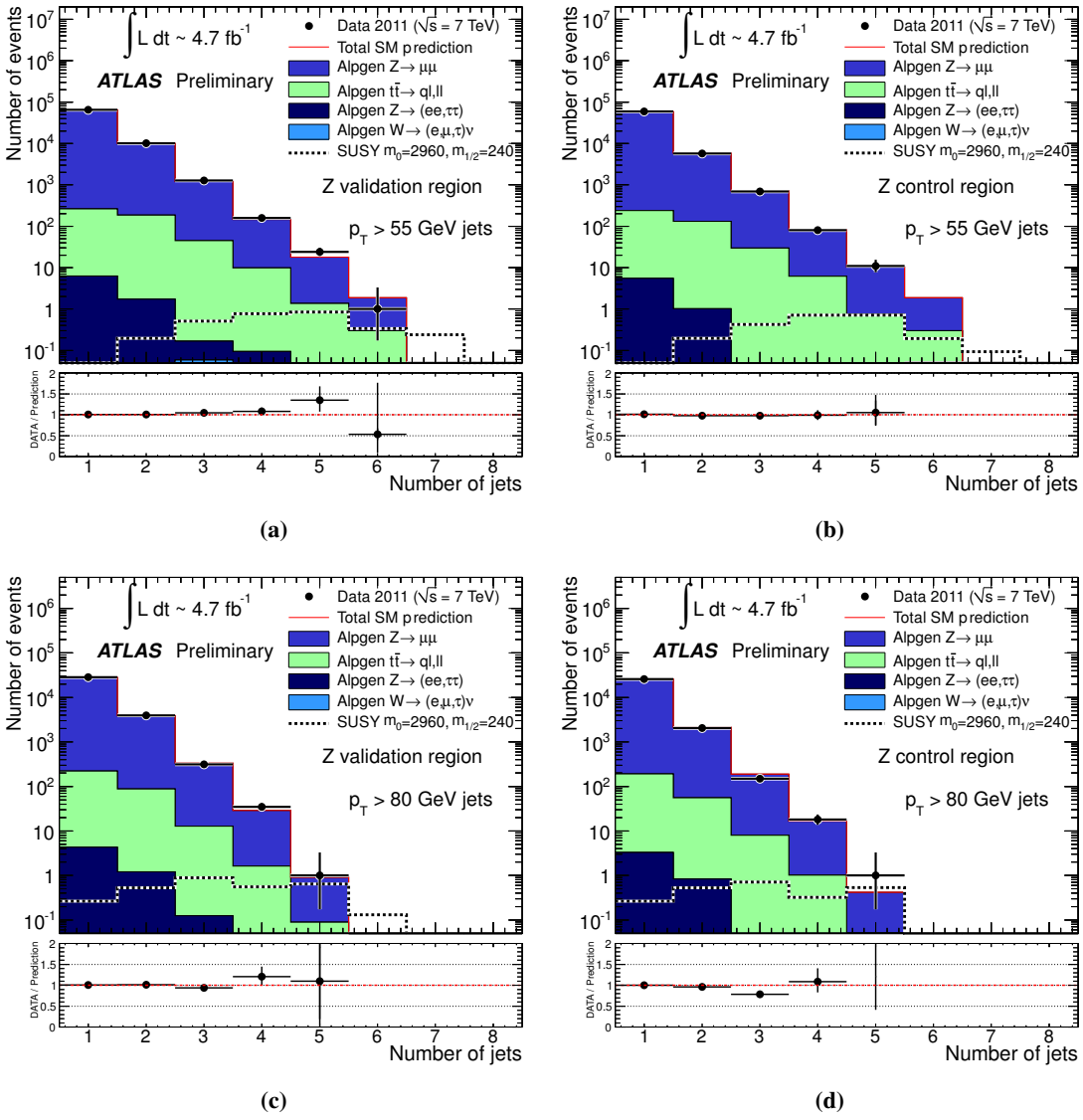

Figure 4: As for Figure 3 but for the Z + jets validation regions and control regions.

Signal region	**7j55**	**8j55**	**9j55**	**6j80**	**7j80**	**8j80**
Multi-jets	91±20	10±3	1.2±0.4	67±12	5.4±1.7	0.42±0.16
$t\bar{t} \to q\ell, \ell\ell$	55±18	5.7±6.0	0.70±0.72	24±13	2.8±1.8	0.38±0.40
W + jets	18±11	0.81±0.72	0+0.13	13±10	0.34±0.21	0+0.06
Z + jets	2.7±1.6	0.05±0.19	0+0.12	2.7±2.9	0.10±0.17	0+0.13
Total Standard Model	**167±34**	**17±7**	**1.9±0.8**	**107±21**	**8.6±2.5**	**0.80±0.45**
Data	**154**	**22**	**3**	**106**	**15**	**1**
$N^{95\%}_{\mathrm{BSM,max}}$ (exp)	72	16	4.5	46	8.4	3.5
$N^{95\%}_{\mathrm{BSM,max}}$ (obs)	64	20	5.7	46	15	3.8
$\sigma^{95\%}_{\mathrm{BSM,max}} \cdot A \cdot \epsilon$ (exp) [fb]	15	3.4	0.96	9.8	1.8	0.74
$\sigma^{95\%}_{\mathrm{BSM,max}} \cdot A \cdot \epsilon$ (obs) [fb]	14	4.2	1.2	9.8	3.2	0.81
p_{SM}	0.64	0.27	0.28	0.52	0.07	0.43

Table 3: Results for each of the six signal regions for an integrated luminosity of 4.7 fb^{-1}. The expected numbers of Standard Model events are given for each of the following sources: multi-jet (including fully hadronic $t\bar{t}$), semi- and fully-leptonic top combined, and W and Z bosons (separately) in association with jets, as well as the total Standard Model expectation. Where small event counts in control regions have not made it possible to determine a central value for the expectation, an asymmetric bound is given instead. The numbers of observed events are also shown. The final five rows show the statistical quantities described in the text. Both the expected (exp) and the observed (obs) values are shown for $N^{95\%}_{\mathrm{BSM,max}}$ and $\sigma^{95\%}_{\mathrm{BSM,max}} \times A \times \epsilon$.

7.1 Systematic uncertainties on 'leptonic' backgrounds

The 'leptonic' background determinations are subject to systematic uncertainties from Monte Carlo modelling of: the jet energy scale (JES, 40%), the jet energy resolution (JER, 4%), the number of multiple proton-proton interactions (3%), the b-tagging efficiency (5% for $t\bar{t}$), the muon trigger and reconstruction efficiency and the muon momentum scale. The numbers in parentheses indicate typical values of the uncertainties for individual Monte Carlo predictions.

The JES and JER uncertainties are calculated using a combination of data-driven and Monte Carlo techniques [23], using the complete 2011 ATLAS data set. The calculation accounts for the variation in the uncertainty with jet p_{T} and η, and that due to nearby jets. The Monte Carlo simulations model the multiple proton-proton interactions with a varying value of $\langle\mu\rangle$ which is well matched to that in the data. The residual uncertainty from pileup interactions is determined by reweighting the Monte Carlo samples so that $\langle\mu\rangle$ is increased or decreased by 10%. The uncertainty in the integrated luminosity is 3.9% [20]. When transfer factors are used to connect control regions to signal regions, the effects of these uncertainties largely cancel in the ratio. For example the residual jet energy scale uncertainty is reduced to $\approx 6\%$.

8 Results, interpretation and limits

Figure 5 shows the $E_{\mathrm{T}}^{\mathrm{miss}}/\sqrt{H_{\mathrm{T}}}$ distributions after applying the jet selections for the six different signal regions (see Table 1) prior to the final $E_{\mathrm{T}}^{\mathrm{miss}}/\sqrt{H_{\mathrm{T}}} > 4$ GeV$^{1/2}$ requirement. Figure 6 shows the jet multiplicity distributions for the two different jet p_{T} thresholds. It should be noted that the signal regions are not exclusive: for example, in Figure 5 all plots contain the same event at $E_{\mathrm{T}}^{\mathrm{miss}}/\sqrt{H_{\mathrm{T}}} \sim 11$ GeV$^{1/2}$. The 'leptonic' backgrounds shown in the figures are those calculated from the Monte Carlo simulation,

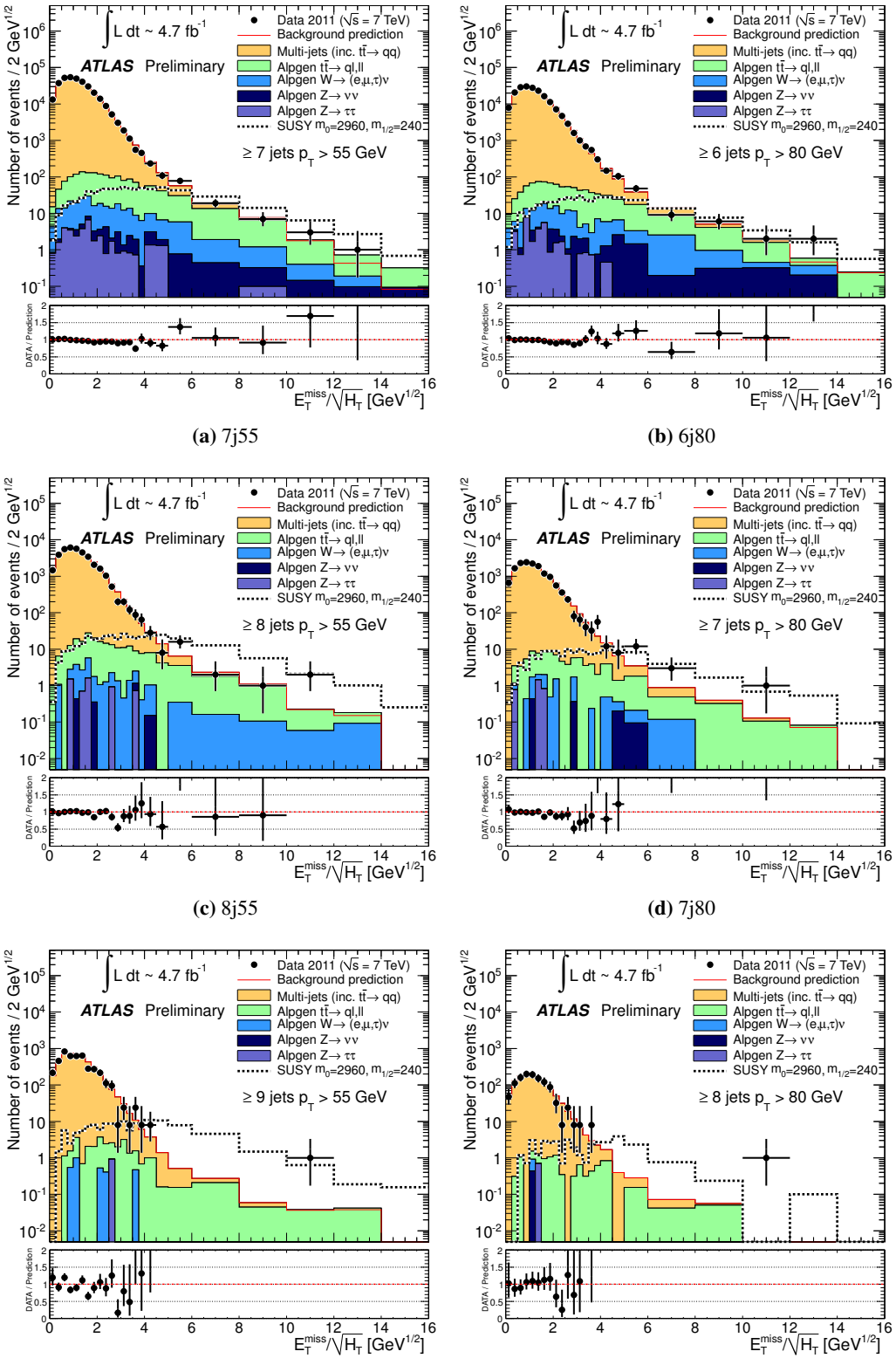

(a) 7j55 **(b)** 6j80

(c) 8j55 **(d)** 7j80

(e) 9j55 **(f)** 8j80

Figure 5: The distribution of the variable $E_{\mathrm{T}}^{\mathrm{miss}}/\sqrt{H_T}$ for each of the six different signal regions defined in Table 1, prior to the final $E_{\mathrm{T}}^{\mathrm{miss}}/\sqrt{H_{\mathrm{T}}} > 4$ GeV$^{1/2}$ requirement.

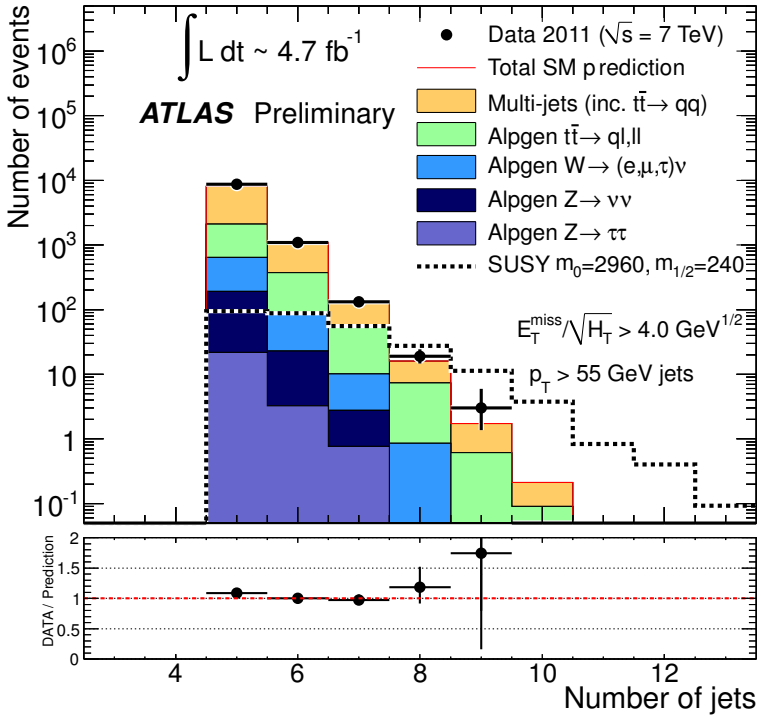

(a)

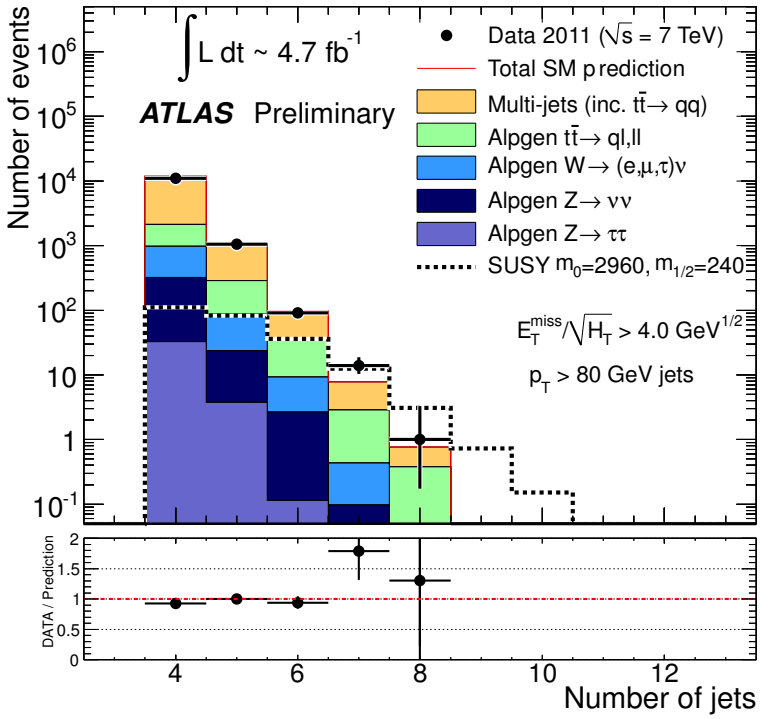

(b)

Figure 6: The distribution of jet multiplicity for jets with p_{T} above 55 GeV **(a)** and those with $p_{\mathrm{T}} >$ 80 GeV **(b)**. Only events with $E_{\mathrm{T}}^{\mathrm{miss}} / \sqrt{H_{\mathrm{T}}} > 4$ GeV$^{1/2}$ are shown.

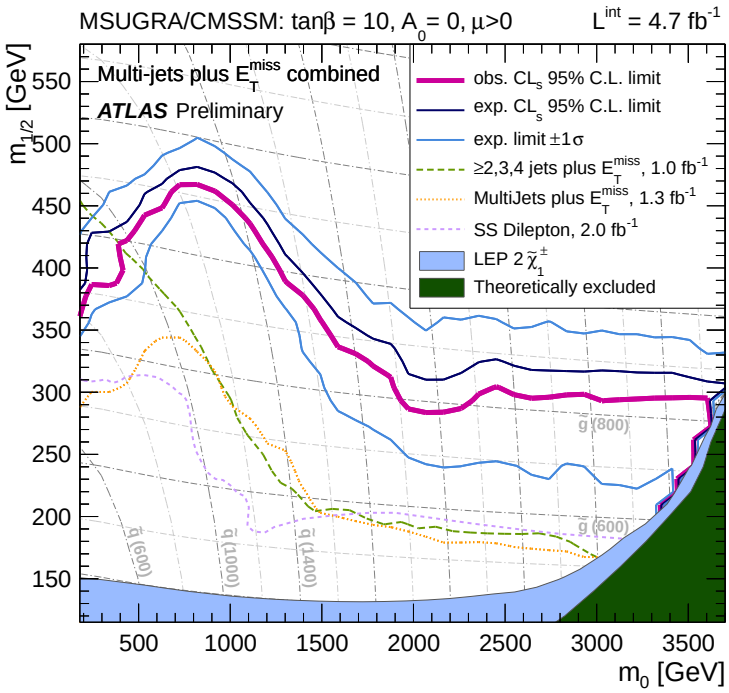

(a) MSUGRA/CMSSM

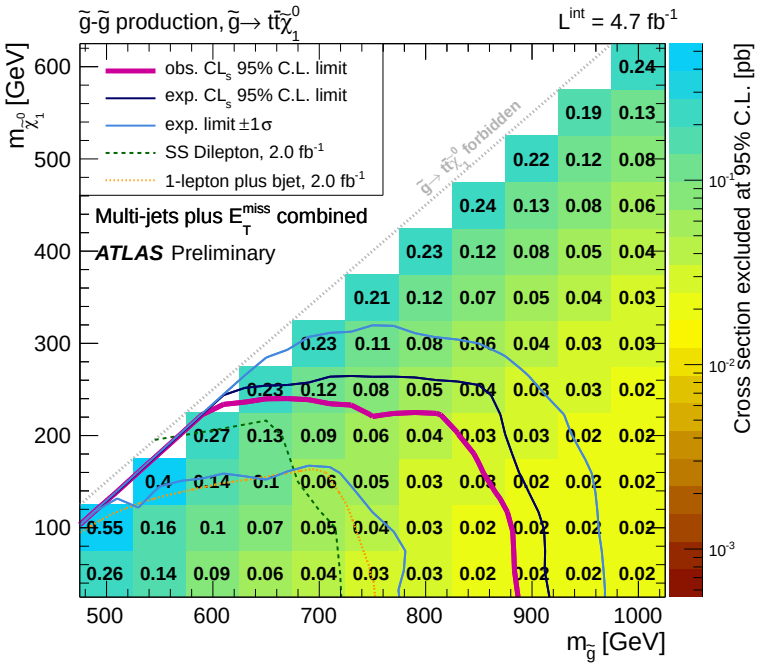

(b) $\tilde{g} - \tilde{\chi}_1^0$ simplified model

Figure 7: Combined 95% C.L. exclusion curves for the $\tan\beta = 10$, $A_0 = 0$ and $\mu > 0$ slice of MSUGRA/CMSSM **(a)** and for the simplified gluino-neutralino model **(b)**. The contours on the MSUGRA/CMSSM model show value of the mass of the gluino and the mean mass of the squarks in the first two generations. The curve for the expected exclusion is also shown, together with its $\pm 1\sigma$ band. The exclusion limits from previous analyses are shown from Refs. [13, 16, 44] **(a)** and from Refs. [45, 44] **(b)**. The colour scale shows the value of $\sigma^{95\%}_{\mathrm{BSM,max}}$ after correction for efficiency and signal acceptance at each point.

using the MC calculation of the cross section and normalised to 4.7 fb^{-1}. The number of events observed in each of the six signal regions, as well as their Standard Model background expectations are shown in Table 3. Good agreement is observed between SM expectations and the data for all six signal regions. Table 3 also shows the 95% confidence level upper bound $N^{95\%}_{\mathrm{BSM,max}}$ on the number of events originating from sources other than the Standard Model, the corresponding upper limit $\sigma^{95\%}_{\mathrm{BSM,max}} \times A \times \epsilon$ on the cross section times efficiency within acceptance (which equals the limit on the observed number of signal events divided by the luminosity) and the p-value for the Standard Model-only hypothesis (p_{SM}).

In the absence of significant discrepancies, limits are set in the context of two supersymmetric (SUSY) models. The first is the $\tan\beta = 10$, $A_0 = 0$ and $\mu > 0$ slice of the MSUGRA/CMSSM parameter space. The second is a simplified SUSY model with only a gluino octet and a neutralino $\tilde{\chi}^0_1$ within kinematic reach. Theoretical uncertainties on the SUSY signals are estimated as described in Section 5. The combined experimental systematic uncertainties from jet energy scale, resolution, and event cleaning are approximately 25%.

The limit for each signal region is obtained by comparing the observed event count with that expected from Standard Model background plus SUSY signal processes, taking into account uncertainties in the expectation, including those which are correlated between signal and background (for instance jet energy scale uncertainties). The combined exclusion regions are obtained using the $\mathrm{CL_s}$ prescription [46], taking the signal region with the best expected limit at each point in parameter space.

The 95% C.L. exclusion in the $\tan\beta = 10$, $A_0 = 0$ and $\mu > 0$ slice of MSUGRA/CMSSM is shown in Figure 7. The analysis substantially extends the previous exclusion limits [13, 16, 17] for $m_0 > 500$ GeV. For large m_0, the analysis becomes independent of the squark mass, and extends the lower bound on the gluino mass to almost 850 GeV for large $m_{\tilde{q}}$. In the simplified model gluinos are pair-produced and decay with unit probability to $t + \bar{t} + \tilde{\chi}^0_1$. In this context, the 95% C.L. exclusion bound on the gluino mass is 880 GeV for neutralino masses up to 100 GeV.

9 Summary

A search for new physics is presented using final states containing large jet multiplicities in association with missing transverse momentum. The search uses the full 2011 pp LHC data-set collected with the ATLAS detector, which corresponds to an integrated luminosity of 4.7 fb^{-1}.

Six non-exclusive signal regions are defined. The first three require at least seven, eight or nine jets, respectively, with $p_{\mathrm{T}} > 55$ GeV; the latter three require at least six, seven or eight jets, respectively, with $p_{\mathrm{T}} > 80$ GeV. In all cases the events are required to satisfy $E^{\mathrm{miss}}_{\mathrm{T}}/\sqrt{H_{\mathrm{T}}} > 4$ GeV$^{1/2}$, and to contain no isolated high p_{T} electrons or muons. By removing the requirement on jet-jet separation used in Ref. [13] the acceptance to signal models of interest is increased by a factor of two to five, without significantly increasing the systematic uncertainty.

The Standard Model multi-jet background is determined using two complementary data-driven methods: firstly a template-based method that exploits the invariance of $E^{\mathrm{miss}}_{\mathrm{T}}/\sqrt{H_{\mathrm{T}}}$ under changes in jet multiplicity, and secondly a jet-smearing method that uses well reconstructed multi-jet seed events from data. The other significant backgrounds — $t\bar{t}$ + jets, W + jets and Z + jets — are determined using a combination of data-driven and Monte Carlo-based methods.

In each of the six signal regions, agreement is found between the Standard Model prediction and the data. In the absence of significant discrepancies, the results are interpreted as limits in the context of R-parity conserving supersymmetry. Exclusion limits are shown for MSUGRA/CMSSM, for which, for large m_0, gluino masses smaller than 850 GeV are excluded at the 95% confidence level. For a simplified supersymmetric model in which both of the pair-produced gluinos decay via the process $\tilde{g} \to t + \bar{t} + \tilde{\chi}^0_1$, gluino masses smaller than about 880 GeV are similarly excluded for $\tilde{\chi}^0_1$ masses up to 100 GeV.

10 Acknowledgments

We thank CERN for the very successful operation of the LHC, as well as the support staff from our institutions without whom ATLAS could not be operated efficiently.

We acknowledge the support of ANPCyT, Argentina; YerPhI, Armenia; ARC, Australia; BMWF, Austria; ANAS, Azerbaijan; SSTC, Belarus; CNPq and FAPESP, Brazil; NSERC, NRC and CFI, Canada; CERN; CONICYT, Chile; CAS, MOST and NSFC, China; COLCIENCIAS, Colombia; MSMT CR, MPO CR and VSC CR, Czech Republic; DNRF, DNSRC and Lundbeck Foundation, Denmark; EPLANET and ERC, European Union; IN2P3-CNRS, CEA-DSM/IRFU, France; GNAS, Georgia; BMBF, DFG, HGF, MPG and AvH Foundation, Germany; GSRT, Greece; ISF, MINERVA, GIF, DIP and Benoziyo Center, Israel; INFN, Italy; MEXT and JSPS, Japan; CNRST, Morocco; FOM and NWO, Netherlands; RCN, Norway; MNiSW, Poland; GRICES and FCT, Portugal; MERYS (MECTS), Romania; MES of Russia and ROSATOM, Russian Federation; JINR; MSTD, Serbia; MSSR, Slovakia; ARRS and MVZT, Slovenia; DST/NRF, South Africa; MICINN, Spain; SRC and Wallenberg Foundation, Sweden; SER, SNSF and Cantons of Bern and Geneva, Switzerland; NSC, Taiwan; TAEK, Turkey; STFC, the Royal Society and Leverhulme Trust, United Kingdom; DOE and NSF, United States of America.

The crucial computing support from all WLCG partners is acknowledged gratefully, in particular from CERN and the ATLAS Tier-1 facilities at TRIUMF (Canada), NDGF (Denmark, Norway, Sweden), CC-IN2P3 (France), KIT/GridKA (Germany), INFN-CNAF (Italy), NL-T1 (Netherlands), PIC (Spain), ASGC (Taiwan), RAL (UK) and BNL (USA) and in the Tier-2 facilities worldwide.

A Event displays

A display of an event that passes the 9j55 and 7j80 signal region selections can be found in Figure 8. A display of an event that passes all signal region selections can be found in Figure 9.

References

[1] P. Fayet, *Supersymmetry and weak, electromagnetic and strong interactions*, *Phys.Lett.* **B64** (1976) 159.

[2] P. Fayet, *Spontaneously broken supersymmetric theories of weak, electromagnetic and strong interactions*, *Phys.Lett.* **B69** (1977) 489.

[3] G. R. Farrar and P. Fayet, *Phenomenology of the production, decay, and detection of new hadronic states associated with supersymmetry*, *Phys.Lett.* **B76** (1978) 575–579.

[4] P. Fayet, *Relations between the masses of the superpartners of leptons and quarks, the goldstino couplings and the neutral currents*, *Phys.Lett.* **B84** (1979) 416.

[5] S. Dimopoulos and H. Georgi, *Softly broken supersymmetry and SU(5)*, *Nucl.Phys.* **B193** (1981) 150.

[6] E. Witten, *Dynamical breaking of supersymmetry*, *Nucl.Phys.* **B188** (1981) 513.

[7] M. Dine, W. Fischler, and M. Srednicki, *Supersymmetric technicolor*, *Nucl.Phys.* **B189** (1981) 575–593.

[8] S. Dimopoulos and S. Raby, *Supercolor*, *Nucl.Phys.* **B192** (1981) 353.

[9] N. Sakai, *Naturalness in supersymmetric GUTs*, *Z.Phys.* **C11** (1981) 153.

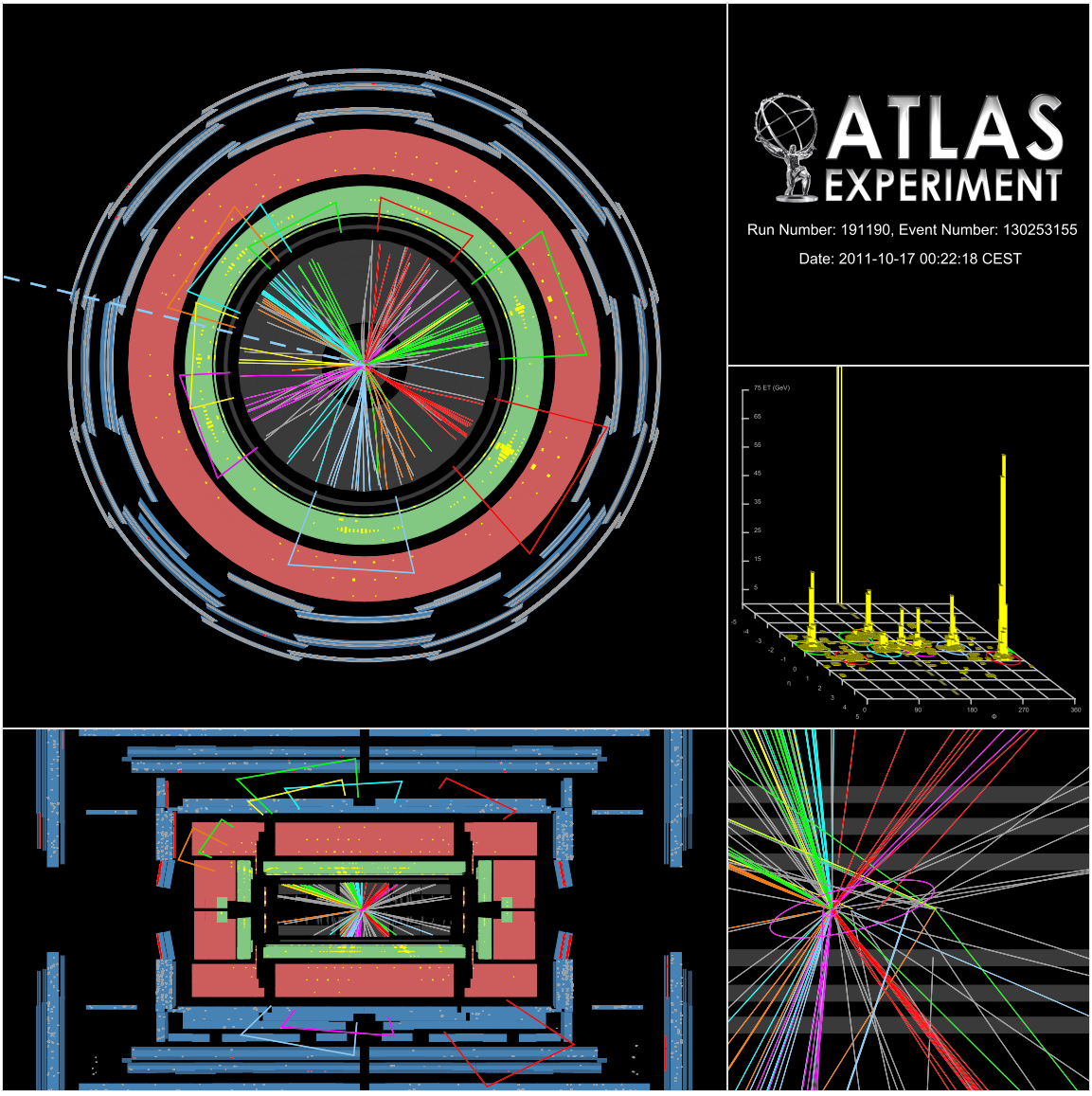

(a)

Figure 8: A display of an event which passes the 9j55 and 7j80 signal region selections. The event has $E_{\mathrm{T}}^{\mathrm{miss}}/\sqrt{H_{\mathrm{T}}}$ of 4.1 $\mathrm{GeV}^{1/2}$ and $E_{\mathrm{T}}^{\mathrm{miss}}$ of 157 GeV.

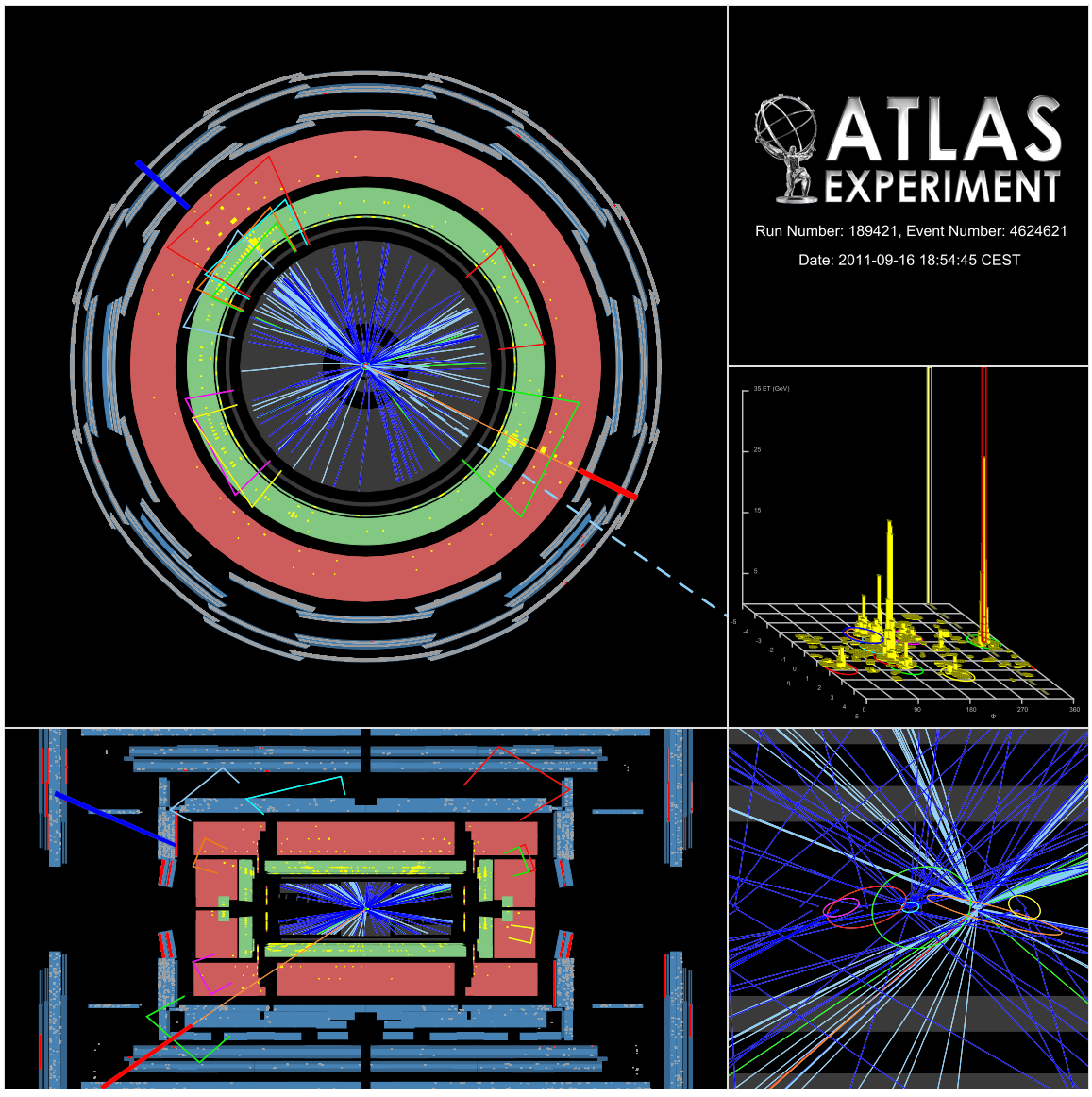

(a)

Figure 9: A display of an event which passes all the signal region selections. The event has $E_{\mathrm{T}}^{\mathrm{miss}}/\sqrt{H_{\mathrm{T}}}$ of 11.6 $\mathrm{GeV}^{1/2}$ and $E_{\mathrm{T}}^{\mathrm{miss}}$ of 397 GeV.

[10] R. K. Kaul and P. Majumdar, *Cancellation of quadratically divergent mass corrections in globally supersymmetric spontaneously broken gauge theories*, *Nucl.Phys.* **B199** (1982) 36.

[11] H. Goldberg, *Constraint on the photino mass from cosmology*, *Phys.Rev.Lett.* **50** (1983) 1419.

[12] J. R. Ellis, J. Hagelin, D. V. Nanopoulos, K. A. Olive, and M. Srednicki, *Supersymmetric relics from the big bang*, *Nucl.Phys.* **B238** (1984) 453–476.

[13] **ATLAS** Collaboration, *Search for new phenomena in final states with large jet multiplicities and missing transverse momentum using $\sqrt{s} = 7$ TeV pp collisions with the ATLAS detector*, *JHEP* **11** (2011) 099, [arXiv:1110.2299].

[14] **ATLAS** Collaboration, *Search for supersymmetry in final states with jets, missing transverse momentum and one isolated lepton in $\sqrt{s} = 7$ TeV pp collisions using 1 fb^{-1} of ATLAS data*, *Phys. Rev.* **D85** (2012) 012006, [arXiv:1109.6606].

[15] **ATLAS** Collaboration, *Searches for supersymmetry with the ATLAS detector using final states with two leptons and missing transverse momentum in $\sqrt{s} = 7$ TeV proton-proton collisions*, arXiv:1110.6189.

[16] **ATLAS** Collaboration, *Search for squarks and gluinos using final states with jets and missing transverse momentum with the ATLAS detector in $\sqrt{s} = 7$ TeV proton-proton collisions*, arXiv:1109.6572.

[17] **ATLAS** Collaboration, *Search for scalar bottom pair production with the ATLAS detector in pp Collisions at $\sqrt{s} = 7$ TeV*, arXiv:1112.3832.

[18] **CMS** Collaboration, *Search for supersymmetry at the LHC in events with jets and missing transverse energy*, *Phys.Rev.Lett.* **107** (2011) 221804, [arXiv:1109.2352].

[19] **ATLAS** Collaboration, *The ATLAS experiment at the CERN Large Hadron Collider*, *JINST* **3** (2008) S08003.

[20] **ATLAS** Collaboration, "Luminosity determination in pp collisions at $\sqrt{s} = 7$ TeV using the ATLAS detector in 2011." ATLAS-CONF-2011-116, Jul, 2011.

[21] M. Cacciari, G. P. Salam, and G. Soyez, *The anti-k_t jet clustering algorithm*, *JHEP* **04** (2008) 063, [arXiv:0802.1189].

[22] M. Cacciari and G. P. Salam, *Dispelling the N^3 myth for the k_t jet-finder*, *Phys. Lett.* **B641** (2006) 57–61, [hep-ph/0512210].

[23] **ATLAS** Collaboration, *Jet energy measurement with the ATLAS detector in proton-proton collisions at $\sqrt{s} = 7$ TeV*, arXiv:1112.6426.

[24] **ATLAS** Collaboration, *Commissioning of the ATLAS high-performance b-tagging algorithms in the 7 TeV collision data*, . ATLAS-CONF-2011-102.

[25] **ATLAS** Collaboration, *Performance of missing transverse momentum reconstruction in proton-proton collisions at 7 TeV with ATLAS*, *Eur.Phys.J.* **C72** (2012) 1844, [arXiv:1108.5602].

[26] M. L. Mangano, M. Moretti, F. Piccinini, R. Pittau, and A. D. Polosa, *ALPGEN, a generator for hard multiparton processes in hadronic collisions*, *JHEP* **07** (2003) 001, [hep-ph/0206293].

[27] J. Pumplin *et. al.*, *New generation of parton distributions with uncertainties from global QCD analysis*, *JHEP* **07** (2002) 012, [hep-ph/0201195].

[28] G. Corcella *et. al.*, *HERWIG 6.5: an event generator for Hadron Emission Reactions With Interfering Gluons (including supersymmetric processes)*, *JHEP* **01** (2001) 010, [hep-ph/0011363].

[29] G. Corcella, I. Knowles, G. Marchesini, S. Moretti, K. Odagiri, *et. al.*, *HERWIG 6.5 release note*, hep-ph/0210213.

[30] J. M. Butterworth, J. R. Forshaw, and M. H. Seymour, *Multiparton interactions in photoproduction at HERA*, *Z. Phys.* **C72** (1996) 637–646, [hep-ph/9601371].

[31] M. Bahr *et. al.*, *Herwig++ physics and manual*, *Eur. Phys. J.* **C58** (2008) 639–707, [arXiv:0803.0883].

[32] W. Beenakker, R. Hopker, M. Spira, and P. M. Zerwas, *Squark and gluino production at hadron colliders*, *Nucl. Phys.* **B492** (1997) 51–103, [hep-ph/9610490].

[33] A. Kulesza and L. Motyka, *Threshold resummation for squark-antisquark and gluino-pair production at the LHC*, *Phys.Rev.Lett.* **102** (2009) 111802, [arXiv:0807.2405].

[34] A. Kulesza and L. Motyka, *Soft gluon resummation for the production of gluino-gluino and squark-antisquark pairs at the LHC*, *Phys.Rev.* **D80** (2009) 095004, [arXiv:0905.4749].

[35] W. Beenakker, S. Brensing, M. Kramer, A. Kulesza, E. Laenen, *et. al.*, *Soft-gluon resummation for squark and gluino hadroproduction*, *JHEP* **0912** (2009) 041, [arXiv:0909.4418].

[36] W. Beenakker, S. Brensing, M. Kramer, A. Kulesza, E. Laenen, *et. al.*, *Squark and gluino hadroproduction*, *Int.J.Mod.Phys.* **A26** (2011) 2637–2664, [arXiv:1105.1110].

[37] P. M. Nadolsky *et. al.*, *Implications of CTEQ global analysis for collider observables*, *Phys. Rev.* **D78** (2008) 013004, [arXiv:0802.0007].

[38] A. Martin, W. Stirling, R. Thorne, and G. Watt, *Parton distributions for the LHC*, *Eur.Phys.J.* **C63** (2009) 189–285, [arXiv:0901.0002].

[39] M. Botje, J. Butterworth, A. Cooper-Sarkar, A. de Roeck, J. Feltesse, *et. al.*, *The PDF4LHC working group interim recommendations*, arXiv:1101.0538.

[40] F. E. Paige, S. D. Protopopescu, H. Baer, and X. Tata, *ISAJET 7.69: A Monte Carlo event generator for pp, $\bar{p}p$, and e^+e^- reactions*, hep-ph/0312045.

[41] **ATLAS** Collaboration, *The ATLAS simulation infrastructure*, *Eur.Phys.J.* **C70** (2010) 823–874, [arXiv:1005.4568].

[42] **GEANT4** Collaboration, S. Agostinelli *et. al.*, *GEANT4: A simulation toolkit*, *Nucl. Instrum. Meth.* **A506** (2003) 250–303.

[43] **ATLAS Collaboration** Collaboration, G. Aad *et. al.*, *Measurement of multi-jet cross sections in proton-proton collisions at a 7 TeV center-of-mass energy*, *Eur.Phys.J.* **C71** (2011) 1763, [arXiv:1107.2092].

[44] **ATLAS** Collaboration, *Search for gluinos in events with two same-sign leptons, jets and missing transverse momentum with the ATLAS detector in pp collisions at $\sqrt{s}$ =7 TeV*, .
ATLAS-CONF-2012-004.

[45] **ATLAS** Collaboration, *Search for supersymmetry in pp collisions at $\sqrt{s} = 7$ TeV in final states with missing transverse momentum and b-jets with the ATLAS detector*, .
ATLAS-CONF-2012-003.

[46] A. Read, *Presentation of search results: the CL_s technique*, *Journal of Physics G: Nucl. Part. Phys.* **28** (2002) 2693–2704.